Vibrational Properties of $RbInSe_2$: Raman Scattering Spectroscopy and First-Principle Calculations

Maxim Guc[1*], Tim Kodalle[2], Ramya Kormath Madam Raghupathy[3], Hossein Mirhosseini[3], Thomas D. Kühne[3], Ignacio Becerril-Romero[1], Alejandro Pérez-Rodríguez[1,4], Christian A. Kaufmann[2], Victor Izquierdo-Roca[1]

[1]Catalonia Institute for Energy Research (IREC), Sant Adrià del Besòs-Barcelona, Jardins de les Dones de Negre 1 2pl., 08930, Spain

[2]Helmholtz-Zentrum Berlin für Materialien und Energie, Schwarzschildstr. 3, 12489 Berlin, Germany

[3]Dynamics of Condensed Matter and Center for Sustainable Systems Design, Chair of Theoretical Chemistry, University of Paderborn, Warburger Str. 100, 33098 Paderborn, Germany

[4]IN^2UB, Departament d'Electrònica, Universitat de Barcelona, Martí i Franquès 1, 08028 Barcelona, Spain

ABSTRACT. $RbInSe_2$ is attracting growing interests as a secondary semiconductor compound in $Cu(In,Ga)Se_2$-based solar cells in virtue of the recent investigations on absorber post-deposition treatments with alkali metal salts that have resulted in significant efficiency improvements. However, the detection of the $RbInSe_2$ phase on the surface of chalcopyrite absorbers is very challenging due to its nanometric thickness and to the limited information available about its fundamental properties. In this context, this work expounds a detailed analysis of the vibrational properties of $RbInSe_2$ that combines first-principle calculations with multiwavelength Raman scattering spectroscopy and provides a methodology for the detection and identification of very thin layers of this material employing solely optical measurements. As a result, we present here the classification of the different vibrational modes together with the fingerprint Raman spectra of $RbInSe_2$ thin films measured under five different excitations (close to and far from resonance). The employment of a 442 nm excitation wavelength is found to be the most adequate strategy for the detection and characterization of the $RbInSe_2$ phase in view of its resonance with the bandgap of the material and its low penetration depth. Additionally, the purity of the deposited thin films as well as the possible influence of the subjacent layers on the Raman spectra of the compound are also investigated by analyzing the presence of secondary phases and by measuring $RbInSe_2$ thin

films deposited onto Mo-coated soda-lime glass, respectively. These results set the basis for the future evaluation of the suitability of Raman spectroscopy as a fast and non-destructive characterization technique for a reliable identification and characterization of the nanometric layers of $RbInSe_2$ in $Cu(In,Ga)Se_2$-based solar cells.

INTRODUCTION

$RbInSe_2$ thin films have recently attracted considerable interest since they may be playing an essential role in the so-called RbF post-deposition treatments (PDTs) carried out on the absorber layer of high efficiency $Cu(In,Ga)Se_2$ (CIGSe) solar cells.[1-4] Alkali-based PDTs have been the driving force boosting the performance of the CIGSe technology in the recent years and have led to a continuous approach of the efficiency of the devices towards the Shockley-Queisser limit.[5-7] However, the origin of the beneficial effects of PDTs on CIGSe devices is still not well-understood and additional research is required to shed light on the underlying mechanisms. The possibility of one of these mechanisms being related to a PDT-induced modification of the surface morphology and composition of the absorber layer is widely discussed. In particular, different groups have shown that the co-evaporation of RbF and Se onto CIGSe absorbers leads to the formation of thin nanometric $RbInSe_2$ layers (as well as of several other compounds such as GaF_3, different oxides and hydroxides) at their surface.[1,3,8-9] However, up to now, the detection and identification of such thin $RbInSe_2$ layers on top of the CIGSe absorbers has required the use of rather advanced characterization techniques like X-ray photoelectron spectroscopy (XPS) or high resolution transmission electron microscopy (TEM).[1,3] In addition, the limited knowledge available regarding the fundamental properties of $RbInSe_2$ further complicates the detection of this phase. To the best of our knowledge, only two publications have investigated the properties of this material through the analysis of either a single crystal[10] or a thin film.[11] In the former article, the authors investigated the crystal structure of a $RbInSe_2$ single crystal processed via the reactive flux method and employed X-ray diffraction (XRD) data to calculate its band structure.[10] In the latter article, the structural (XRD) and optical (UV-Vis measurements) properties of a thermally co-evaporated $RbInSe_2$ thin film were analyzed.[11] In addition, the phase formation energies of the different species in the Rb-In-Se system as well as the possible intrinsic defects in $RbInSe_2$ were discussed based on first-principle calculations. These works have revealed that $RbInSe_2$ crystallizes in a monoclinic Bravais lattice where two-dimensional layers are separated by Rb^+ cations[10] and that

this material has a direct 2.8 eV bandgap with a relatively high absorption coefficient above the absorption edge (> 10^4 cm^{-3}).[11]

In this context, this work investigates the vibrational properties of $RbInSe_2$ thin films employing multiwavelength Raman scattering spectroscopy in order to obtain the fingerprint spectra of the material and set the basis for the future evaluation of the suitability of Raman spectroscopy as a fast and non-destructive characterization technique for a reliable detection, identification and characterization of very thin layers of $RbInSe_2$ in $Cu(In,Ga)Se_2$-based solar cells. The experimental results are correlated with first-principle calculations, which allows the classification of the vibrational modes of $RbInSe_2$. Furthermore, the homogeneity and phase purity of the $RbInSe_2$ thin films are assessed by means of Raman spectroscopy by investigating the presence of possible secondary phases. Finally, the influence of a $MoSe_2$ subjacent layer on the Raman spectra is also analyzed.

EXPERIMENTAL DETAILS

$RbInSe_2$ thin films were deposited onto soda-lime glass (SLG) substrates using a one-stage thermal co-evaporation process. Some of the substrates were coated with an 800 nm thick Mo layer deposited by DC-sputtering. Elemental Se and In as well as RbF were evaporated onto the substrates from separate sources in order to be able to adjust the evaporation rates to obtain the desired composition of the thin film. The substrate temperature was set to 550 °C. After finishing the deposition process, all the samples were rinsed in diluted ammonia to wash off possible residues of fluorine compounds and excess Rb. A more detailed description of the deposition procedure can be found in Ref. 11. The results on detailed structural, compositional and morphological analysis of the thin films used for the experimental study below were also presented in Ref. 11. Note that the present study was carried out with a samples from the very the same deposition run as the sample characterized in Ref. 11 ensuring the applicability of the results of that study to the samples discussed in the present study.

Raman scattering spectra were acquired using a FHR640 and an *i*HR320 spectrometer (Horiba Jobin-Yvon) coupled to a CCD detector and optimized for the UV-Vis and near IR spectral regions, respectively. The measurements were performed in backscattering configuration through an Olympus objective coupled to a special probe designed at IREC. The excitation was performed using solid-state (532 and 785 nm) and gas (325, 442 and 632.8 nm) lasers. The dependence of the

spectra with the laser power density was analysed for each excitation laser line and the highest energy without an influence on the sample was selected for the subsequent study (values around 25 W/cm^2 were used in most cases). The excitation laser lines were selected taking into account the band gap of $RbInSe_2$ (2.8 eV[11] which corresponds to 442 nm) so that three of them had energies below the bandgap (785, 632.8 and 532 nm), one had a higher energy (325 nm) and one perfectly matched the bandgap energy leading to resonant conditions (442 nm). Such multiwavelength excitation analysis has allowed obtaining fingerprint Raman spectra measured under different conditions which can be used as a reference in the further analyses of the $RbInSe_2$ compound.

LATTICE DYNAMICS CALCULATIONS

The Raman scattering spectrum of the $RbInSe_2$ crystal structure has been calculated from the first-principles lattice-dynamics calculations as implemented within the Vienna *ab* initio simulation package (VASP).[12] Structural optimization has been performed using the Perdew, Burke, and Ernzerhof (PBE) generalized gradient approximation functional.[13] A plane-wave cut-off of 520 eV and a Γ-centred (2x2x2) k-point mesh have been employed. The projector augmented wave (PAW)[14] potentials used in the calculations were constructed so that they treated the (4s2 4p6 5s1), (5s2 5p1), and (4s2 4p4) shells as valence states for Rb, In and Se, respectively. The calculations were carried out on a 64-atom supercell. The calculated lattice parameters for the $RbInSe_2$ compound are in close agreement with the experimental lattice parameters (a = 11.502 Å, b = 11.496 Å, c = 16.469 Å).[11] Hence, the latter were chosen for the spectral calculations. Internal structural parameters were converged to within 10^{-8} eV or until the magnitude of the forces on the ions were below 10^{-3} eV/Å for the phonon calculations. The off-resonant Raman activity calculator was used to determine the derivative of the polarizability (or macroscopic dielectric tensor) with respect to the normal mode coordinate: dP/dQ.[15]

Table 1. *Raman scattering one-phonon peaks of $RbInSe_2$ obtained from first-principle calculations and the analysis of the experimental spectra.*

No.	Calculations	Experimental	
	Raman shift (cm^{-1})	Raman shift (cm^{-1})	FWHM (cm^{-1})
1	4.7		
2	17.0		
3	22.8		
4	43.8		
5	47.0		
6	57.8		
7	61.6		
8	69.9		
9	71.0		
10	78.4	79.5	4.5
11	89.5	90.5	5.0
12	92.8	95.1	5.9
13	99.1		
14	102.0	102.6	7.7
15	**113.05**	**114.3**	**5.5**
16	**175.8**	**179.7**	**6.1**
17	181.0		
18	183.7	186.9	6.3
19	195.6	198.0	7.2
20	201.8		
21	203.7	203.3	7.9
22	222.3	211.2	10.1
23	228.5	224.4	7.0
24	**237.9**	**238.0**	**6.5**

$RbInSe_2$ has a monoclinic structure with space group $C2/c$ and 16 atoms in the primitive cell, similar to the $TlGaSe_2$ structure.[16] Group theory analysis yields 48 phonons in the zone centre Γ-point, which are collected in the following irreducible representation:[17]

$$\Gamma = 10A_g \oplus 10A_u \oplus 14B_g \oplus 14B_u, \quad (1)$$

where $A_u \oplus 2B_u$ are the acoustic modes and the rest are optic modes split into $9A_u \oplus 12B_u$ infrared and $10A_g \oplus 14B_g$ Raman active modes.[17] This way, up to 24 peaks are expected in the Raman spectra of $RbInSe_2$. The calculated frequencies of the Raman modes and their symmetries are presented in Table 1. A Lorentzian instrumental broadening was applied to simulate the Raman spectrum and a good matching was observed with the experimental spectra (Figure 1a) as will be discussed below.

EXPERIMENTAL RESULTS AND DISCUSSIONS

Raman scattering analysis. The Raman scattering spectra of the $RbInSe_2$ thin films measured under the different excitation wavelengths (except for the one obtained with the 325 nm laser) are presented in Figure 1b. A good correlation can be observed between the experimental spectra and the one obtained from first-principles calculations (Figure 1a), even in the relative intensity of the different peaks. The main difference between them, though, lies in the band close to 150 cm^{-1} detected in the three spectra measured with excitation wavelengths corresponding to energies below the bandgap of $RbInSe_2$ (785, 632.8 and 532 nm) which is not present in the calculated spectrum. This issue will be discussed later on. Besides sharing the presence of the band at 150 cm^{-1}, the three spectra measured with excitation energies below the bandgap of $RbInSe_2$ look quite similar and display comparable relative intensities of all the peaks. In contrast, the spectrum measured under a blue (442 nm) excitation wavelength (i.e. under resonant conditions) exhibits an increased intensity in the peak located at 115 cm^{-1} and lower intensity in the peak at 239 cm^{-1}. Note that the overall shape of the Raman spectra of $RbInSe_2$ measured under resonant conditions is also similar to the spectra of the $RbGaSe_2$ compound.[18] However, the vibration frequencies in the gallium containing compound show a blue shift of about 15 – 40 cm^{-1}, which indicates stronger In–Se bonding interactions in $RbInSe_2$ compared to $RbGaSe_2$. Interestingly, the band detected at 150 cm^{-1} is observed to disappear in this spectrum whereas the peaks in the 190 – 230 cm^{-1} range became more pronounced. These changes in the relative intensity of the peaks are related to the

way in which the different types of vibrations, longitudinal or transversal, that originate such peaks interact with the excitation light. As the excitation light approaches resonance, the peaks associated with longitudinal vibrations became more intense than those associated with transversal vibrations due to the Fröhlich electron−phonon interaction.[19] Additionally, owing to the different resonance conditions of the secondary phases and the main phase, the intensity of their corresponding peaks may vary in a different way when changing the excitation wavelength which also contributes to the observed differences. In fact, the employment of multiwavelength excitation has been shown to be a powerful technique for the detection of secondary phases in complex compounds like kesterites.[20]

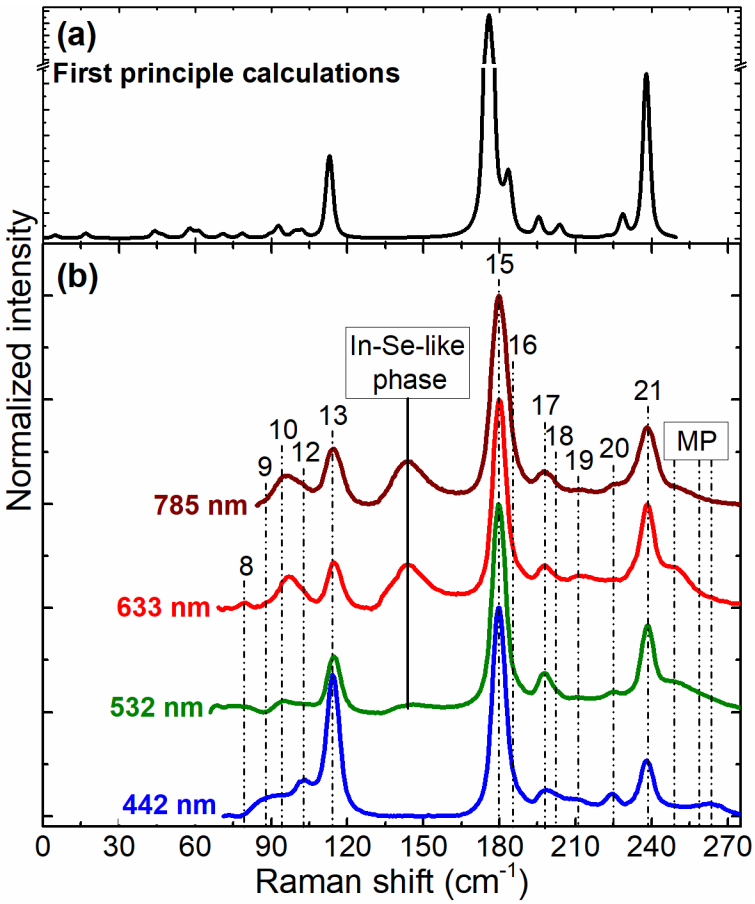

Figure 1. *(a) Calculated Raman scattering spectra of $RbInSe_2$. A break was made in the Y-axis to elucidate the low intensity peaks. (b) Raman scattering spectra of $RbInSe_2$ thin films deposited on SLG substrate measured under different excitation wavelengths. MP denotes the multi-phonon peaks. The numbers on the peaks correspond to those shown in Table 1.*

On the other hand, the measurements carried out under UV (325 nm) excitation wavelength show a high dependence on laser power density. A broad band at around 250 cm^{-1} is detected even with the lowest possible power density (close to 0.3 W/cm^2). Increasing this value up to ~3 W/cm^2 leads to a clear evolution of the spectra with time in which the intensity of the peak at 254 cm^{-1}, which is related to the amorphous Se phase,[21] keeps rising (see Figure 2). This denotes an easy decomposition of the $RbInSe_2$ compound under UV excitation. However, it should be noted that the lowest power density employed (0.3 W/cm^2) is already more than one order of magnitude higher than the average power density of the UV part of the solar spectrum (AM 1.5).

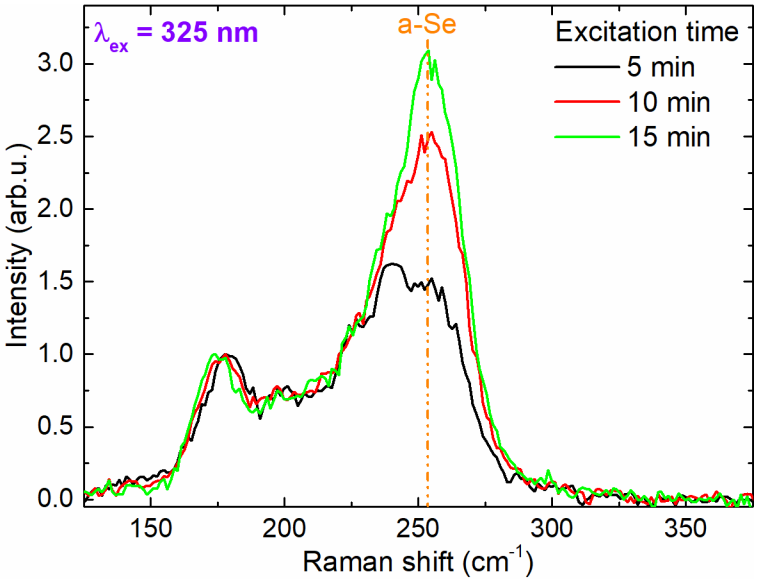

Figure 2. *Evolution of the Raman scattering spectra of $RbInSe_2$ with the UV excitation time.*

A simultaneous deconvolution of the Raman scattering spectra of $RbInSe_2$ measured under different excitation wavelengths into individual Lorentzian peaks was performed. As an example, the spectrum measured under blue laser (442 nm) excitation is presented in Figure 3. This deconvolution methodology has been previously applied to the analysis of different materials,[22-24] enabling the resolution of low intensity and highly overlapped peaks. Here, the positions of all the peaks found for $RbInSe_2$ from the proposed deconvolution of the broad bands are collected in Table 1. Although small discrepancies exist between the frequency of the calculated and the experimentally measured vibrational modes, these are below 5 cm^{-1} in all cases. This indicates that the initial parameters and the model employed are well-suited for the calculations performed in this work. Table 1 also shows the full widths at the half maximum (FWHM) of the different peaks.

The relatively low FWHM values suggest that the analyzed thin film possesses a good crystalline quality. An exception is observed in the peak located at 211.2 cm^{-1} which exhibits a higher-than-average FWHM. This can be related to the overlapping of various peaks at this spectral position that are not fully resolved during the deconvolution. It should be noted that, in addition to the one-phonon peaks collected in Table 1, a series of multiphonon (MP) peaks were also detected, mainly in the spectra measured under resonant conditions (442 nm excitation) (see Figure 1b). These peaks are presented in Table 2 with their possible decipherment to the constituent one-phonon modes.

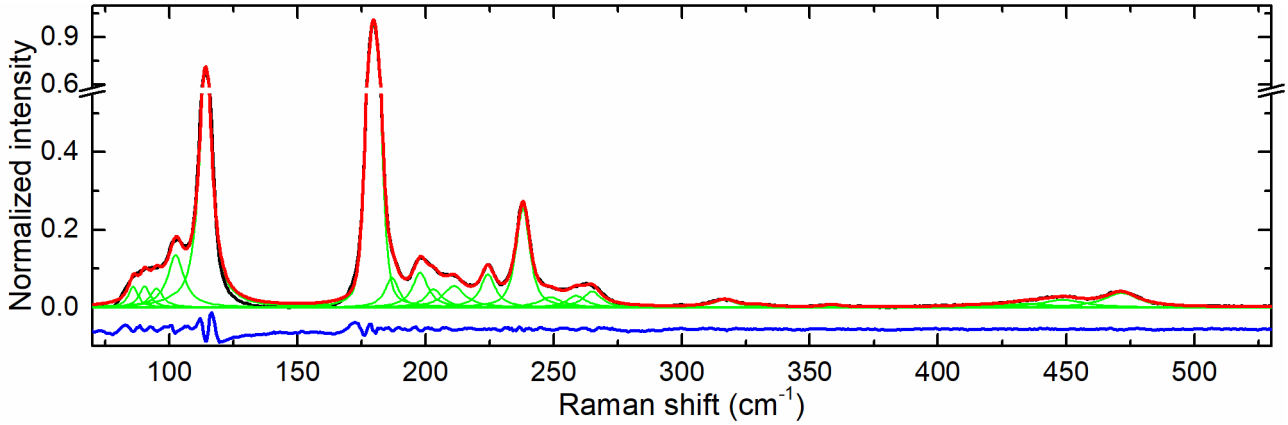

Figure 3. *Fitting (red curves) of the experimental Raman spectrum (black curves) of $RbInSe_2$ using Lorentzian functions (green curves). The difference between the fitted and experimental spectra are shown with the blue curve. The spectrum was measured under 442 nm excitation wavelength. The break in the Y axis has been included to emphasize the low intensity peaks.*

Table 2. *Multiphonon peaks found in the Raman scattering spectra of $RbInSe_2$ measured under resonant 442 nm excitation wavelength.*

Raman shift (cm^{-1})	FWHM (cm^{-1})	Decipherment
249	10.9	*71.0*+179.7
259	9.0	*22.8*+238.0
265	8.4	79.5+179.7
317	11.6	79.5+238.0
330	8.5	90.5+238.0
359	7.3	179.9×2
415	24.0	179.9+238.0
435	22.1	198.0+238.0
449	19.9	211.2+238.0
471	16.3	238.0×2

Secondary phases. According to previous results, the formation energy of the ternary $RbInSe_2$ compound is comparable to the formation energies of different binary compounds.[11] As such, the formation of secondary phases along with the main $RbInSe_2$ phase during the synthesis process can be expected. Among the different possible secondary phases, In-Se based and Rb-Se based compounds are the most likely to be formed.[11] Additionally, as observed in the Raman spectra measured under UV excitation, peaks related to elemental Se can also appear in the spectra.

Regarding Rb-Se compounds, only very limited information can be found in the literature. The published works mainly cover the experimental investigation[25,26] and first-principle calculations[11,27,28] of their structural, electronic, and optical properties. However, no information about the Raman spectra of Rb-Se compounds has been published, which complicates the investigation of their possible influence on the Raman analysis of $RbInSe_2$. However, since the investigated thin films were deposited under the same technological conditions described in,[11] where the analysis of XRD patterns did not show the presence of any Rb-Se compound, we can assume the absence of these secondary phases in our samples, too.

In the case of the In-Se system, different structural and compositional polymorphs are expected. Interestingly, most of them present their main Raman peak in the 100 – 150 cm^{-1} range.[29-33] Thus, this observation suggests that the band found at 150 cm^{-1} in the spectra measured in this work is probably originating from compounds related to In-Se phases. However, the two constituents peaks (at 145 and 153 cm^{-1}) found for this broad band do not strictly correspond to any compound from the In-Se system such as α-In_2Se_3, γ-In_2Se_3, InSe or $InSe_2$ whose main Raman peaks are located at 104, 151, 114 and 150 cm^{-1}, respectively.[29-31,33] This points towards the 150 cm^{-1} band being formed by a mixture of different structural and compositional polymorphs and/or amorphous In-Se secondary phases which strongly complicates their detection and analysis by XRD. Moreover, these phases were not detected in the previously published X-ray diffractograms of the $RbInSe_2$ layer[11] despite being detected in the Raman spectra presented here. The non-intrinsic nature of this band at 150 cm^{-1} is in agreement both with the first-principle calculations of the Raman modes of $RbInSe_2$ presented above and with its rising intensity with the increasing excitation wavelength. What is more, different species in the In-Se system have a lower bandgap than $RbInSe_2$ (in the range 1.2 – 2.4 eV, depending on their composition and structure)[31-33] which

can match with some of the excitation wavelengths employed (532, 632.8 and 785 nm) leading to resonant or close to resonant measuring conditions and profoundly enhancing the intensity of their Raman signal. This could explain the clear presence of the 150 cm^{-1} band in the spectra obtained in this work for such excitation wavelengths. However, it should be noted that working under resonant conditions enables the detection of residually small amounts of secondary phases,[34] which means that the presence of In-Se based secondary phases in the sample analyzed here is almost negligible. Oppositely, in case of the 442 nm excitation laser, the strong resonance of this wavelength with the bandgap of $RbInSe_2$ phase highly increases the intensity of its Raman peaks in comparison with those belonging to the In-Se secondary phases resulting in the disappearance of the band at 150 cm^{-1}. Therefore, it can be concluded that the 442 nm excitation wavelength is the most suitable one for the analysis of the $RbInSe_2$ phase without interferences from the peaks of possible secondary phases.

Alongside with the sample deposited on SLG, a sister sample was deposited on a Mo-coated SLG substrate. Figure 4a shows the Raman spectra measured under different excitation wavelengths. Some differences with respect to the spectra shown in Figure 1 are observed. The main difference can be spotted in the spectrum measured under a 785 nm excitation wavelength where a peak at 291 cm^{-1} appears. This peak is related to the $MoSe_2$ phase,[35] which is expected to form at the Mo/$RbInSe_2$ interface. It should be noted, though, that the most intense $MoSe_2$-related peak[35] is expected at 242 cm^{-1} so it strongly overlaps with the peaks of the main $RbInSe_2$ phase located at 238 cm^{-1}. An asymmetric broadening of the band at 240 cm^{-1} is observed in all the spectra measured under excitation wavelengths lower than the bandgap of $RbInSe_2$ (532, 632.8 and 785 nm) which could further confirm the presence of the $MoSe_2$ phase. In order to study this, we compared the differences in Raman shift and FWHM of the band at 240 cm^{-1} for the thin films deposited on bare SLG and on Mo-coated SLG (Figure 4b and 4c). A sharp shift of the band towards higher wavenumbers is detected in the thin film deposited on SLG/Mo for excitation wavelengths $\geq$ 532 nm (Figure 4b). The relative FWHM of the band at 240 cm^{-1} was calculated as the ratio of the width of this band and the width of the main peak of $RbInSe_2$, which allows avoiding the crystalline inhomogeneities and instrument limitations. This value was found to be higher in the spectra of the sample deposited on SLG/Mo excited with 532 and 632.8 nm wavelengths while it is comparable to that of the bare SLG sample for 442 and 785 nm excitations. The latter is probably related to the intensity rise of the $MoSe_2$ peak at 242 cm^{-1} which becomes

the dominant one, while the peak at 238 cm^{-1} from $RbInSe_2$ becomes a shoulder and does not introduce any significant broadening to the band.

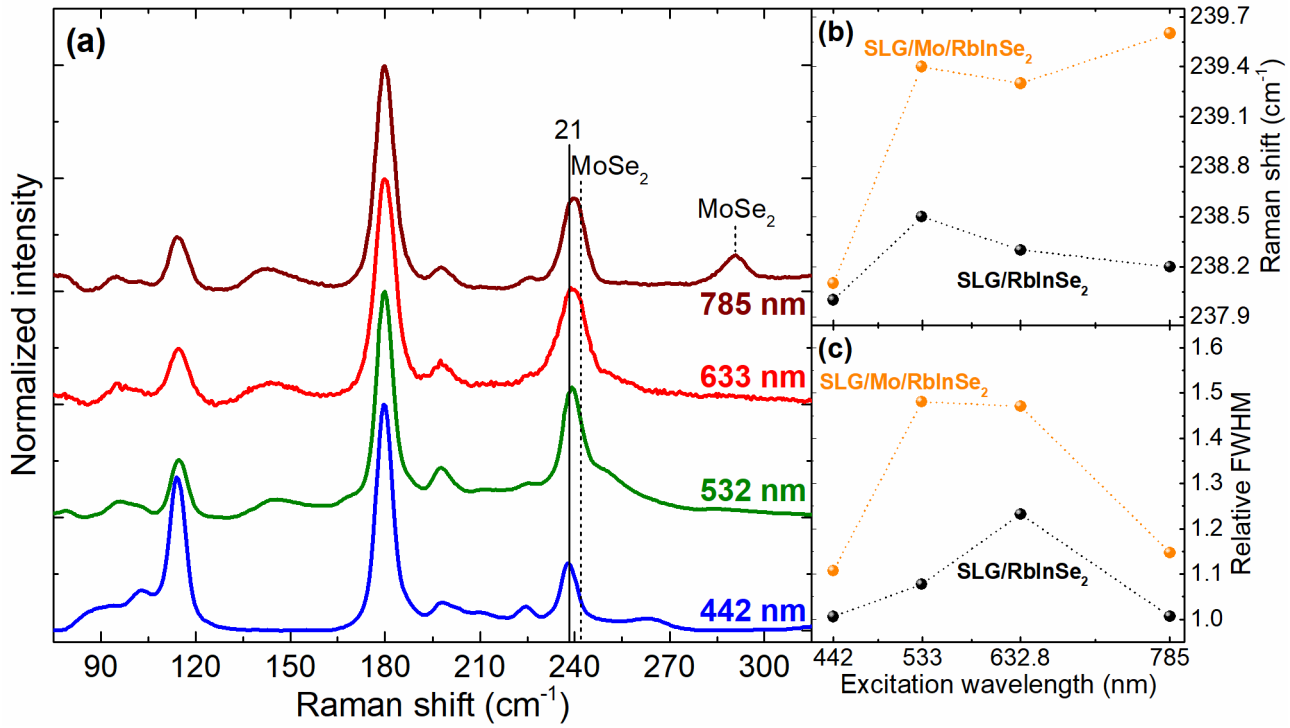

Figure 4. *(a) Raman scattering spectra of $RbInSe_2$ thin films deposited on Mo coated SLG substrate excited with different laser wavelengths. (b) Evolution of the Raman shift of the band close to 240 cm^{-1} with excitation wavelength. (c) Evolution of the relative FWHM (calculated as a ratio of the FWHM of the band and main peak of $RbInSe_2$) of the band close to 240 cm^{-1} with excitation wavelength.*

To gain a deeper insight, additional measurements of the Raman spectra of the thin films deposited on Mo-coated SLG substrate were performed under the resonant blue excitation wavelength after a mechanical lift-off of the $RbInSe_2$ layer and are shown in Figure 5. The lift-off approach has been widely employed for the analysis of the interfaces in other chalcogenide materials.[36-41] No differences are found in the spectra measured at the front and back sides of the $RbInSe_2$ layer (top of Figure 5). On the other hand, the spectrum measured at the substrate in the lifted-off region is similar to the reference spectra of $MoSe_2$ phase (bottom of Figure 5). This proves the formation of a $MoSe_2$ phase at the Mo/$RbInSe_2$ interface. The fact that $MoSe_2$ is also clearly observed in the spectra of the full samples measured at the top of the thin film with the 532, 632.8 and 785 nm excitation wavelengths is related to the high penetration of these lasers through the high bandgap $RbInSe_2$ layer reaching the back interface. Moreover, using the data of spectral dependence of the

absorption coefficient of $RbInSe_2$,[11] it is possible to estimate that the penetration depth of these excitation wavelengths is ≥1 μm. This analysis shows that the subjacent layers can influence the Raman spectra of $RbInSe_2$ when employing excitation laser with energies lower than the bandgap of this compound. On the contrary, it is also possible to estimate from the same data that the penetration depth of the resonant blue laser is not exceeding 100 nm. Thus, the $RbInSe_2$ phase can be detected from a small amount of material further confirming that the 442 nm excitation wavelength is the most suitable one for detection of the $RbInSe_2$. In this regard, shifting to UV excitation wavelengths should be even more sensitive, reducing the penetration depth down to a few tens of nm. However, as it has been shown in the present study, the employment of UV excitation leads to the decomposition of the $RbInSe_2$ layer, even at very low power densities.

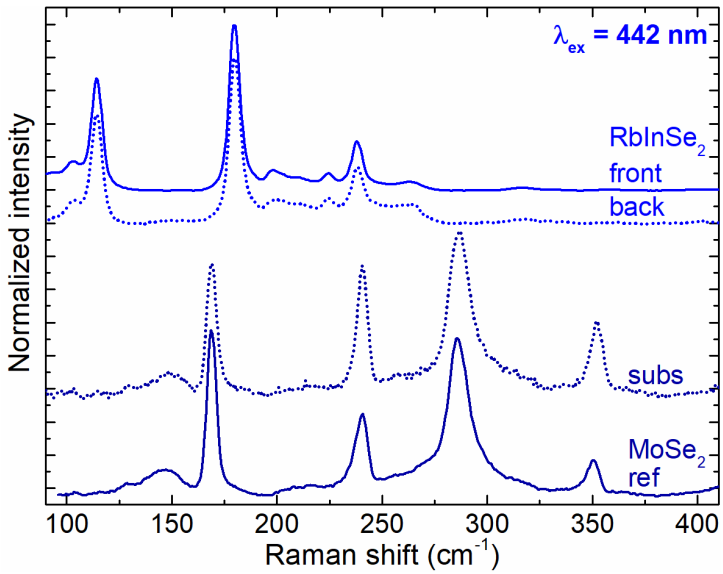

Figure 5. *Raman scattering spectra of $RbInSe_2$ thin film deposited on a Mo coated SLG substrate measured from the front and back of the layer, after mechanical lift-off, under blue excitation wavelength. Spectra measured at the lifted-off region of the sample (subs) and the $MoSe_2$ reference (ref) spectra are presented at the bottom of the graph.*

Taking into account the findings presented above of the possible overlap of the Raman peaks of $RbInSe_2$, with the peaks from subjacent layers, and in connection with the possible application of the presented Raman spectra for a reliable identification and characterization of nanometric $RbInSe_2$ layers on top of $Cu(In,Ga)Se_2$ absorbers, it is worth to make a comparison of the peaks present in the Raman spectra of these two compounds. A typical Raman spectrum of $CuInSe_2$ has a high intensity peak at 173-175 cm^{-1}, and several less intense peaks (< 10% of the main peak

intensity outside of the resonant conditions) in the low wavenumber range below 80 cm^{-1} and in the high wavenumber range above 200 cm^{-1}.[42-44] The latter peaks are not expected to have significant influence on the detection of $RbInSe_2$ while the main peak of $CuInSe_2$ can overlap with the main peak of $RbInSe_2$ at 180 cm^{-1}. The detection of $RbInSe_2$ can become even more complex in the case of $Cu(In,Ga)Se_2$ absorbers, where Ga incorporation leads to a shift of the main peak of the compound to higher wavenumbers and therefore closer to the main peaks of $RbInSe_2$.[45,46] Taking into account that the expected thickness of the RbInSe2 layer on top of a post-deposition treated $Cu(In,Ga)Se_2$ absorber is nanometric (< 10 nm),[1] the intensities of the $RbInSe_2$-related Raman peaks are not expected to be high even under resonant conditions. In this case, it can appear that the main peak of $RbInSe_2$ will exhibit only a shoulder at the high wavenumber side of the main CIGSe peak. This could create a problem for the detection of $RbInSe_2$ based on the main Raman peak of this compound. However, the second most intense peak at 114 cm^{-1} measured under resonant excitation conditions (442 nm) is not overlapped with any of the peaks of the CIGSe compounds,[42-46] and has an intensity only 25% lower than that of the main peak. Under these conditions, the appearance of the peak at 114 cm^{-1} in the Raman spectra of a CIGSe compound after a PDTs measured under 442 nm excitation can be a direct evidence of $RbInSe_2$ formation. However, this should be checked in further experimental work.

CONCLUSIONS

To conclude, an elaborate analysis of the vibrational properties of $RbInSe_2$ thin films has been performed employing first-principle calculations and multiwavelength Raman scattering spectroscopy. We presented the classification of the different vibration modes and the fingerprint Raman spectra of $RbInSe_2$ measured under different (resonant and off-resonance) excitation conditions. The fine fitting of such spectra allowed finding 12 out of the 24 possible Raman peaks with frequencies close to those corresponding to the calculated vibrational modes. Furthermore, a detailed analysis of the influence of possible secondary phases and subjacent layers on the Raman spectra of $RbInSe_2$ was performed. This led to the detection of a band that corresponds to In-Se like secondary phases and, in the case of $RbInSe_2$ layers fabricated on SLG/Mo, to the observation of peaks attributed to $MoSe_2$. From these analyses, it has been shown that the employment of a 442 nm excitation wavelength is the most suitable strategy for the investigation and detection of the $RbInSe_2$ phase by Raman spectroscopy since its resonance with the bandgap of $RbInSe_2$ avoids

interferences from possible secondary phases and its low penetration depth makes the measurements independent from the subjacent layers.

AUTHOR INFORMATION

*Corresponding author. E-mail: mguc@irec.cat

The authors declare no competing financial interests.

ACKNOWLEDGEMENTS

The authors would like to thank B. Bunn and K. Mayer-Stillrich for the preparation of the Mo-covered SLG substrates. This research was supported by the H2020 Programme under the project INFINITE-CELL (H2020-MSCA-RISE-2017-777968), by the Spanish Ministry of Science, Innovation and Universities under the WINCOST (ENE2016-80788-C5-1-R), and by the European Regional Development Funds (ERDF, FEDER Programa Competitivitat de Catalunya 2007–2013). Authors from IREC and the University of Barcelona belong to the SEMS (Solar Energy Materials and Systems) Consolidated Research Group of the "Generalitat de Catalunya" (Ref. 2017 SGR 862). The authors would like to acknowledge financial support from the German Bundesministerium für Wirtschaft und Energie (BMWi) for the speedCIGS project (0324095C and 0324095D). RKMR, TDK, and HM would like to acknowledge the Paderborn Center for Parallel Computing (PC 2) for computing time on OCuLUS and FPGA-based supercomputer NOCTUA. MG This project has received funding from the European Union's Horizon 2020 research and innovation programme under the Marie Skłodowska-Curie grant agreement No 712949 (TECNIOspring PLUS) and the Government of Catalonia's Agency for Business Competitiveness(ACCIÓ).

REFERENCES

[1] Taguchi, N.; Tanaka, S.; Ishizuka, S. Direct Insights into $RbInSe_2$ Formation at $Cu(In,Ga)Se_2$ Thin Film Surface with RbF Postdeposition Treatment. Appl. Phys. Lett. 2018, 113, 113903.

[2] Ishizuka, S.; Taguchi, N.; Nishinaga, J.; Kamikawa, Y.; Tanaka, S.; Shibata, H. Group III Elemental Composition Dependence of RbF Postdeposition Treatment Effects on $Cu(In,Ga)Se_2$ Thin Films and Solar Cells. J. Phys. Chem. C 2018, 122, 3809-3817.

[3] Kodalle, T.; Heinemann, M. D.; Greiner, D.; Yetkin, H. A.; Klupsch, M.; Li, C.; van Aken, P. A.; Lauermann, I.; Schlatmann, R.; Kaufmann, C. A. Elucidating the Mechanism of an RbF Post Deposition Treatment in CIGS Thin Film Solar Cells. Solar RRL 2018, 2, 1800156.

[4] Malitckaya, M.; Komsa, H.-P.; Havu, V.; Puska, M. J. Effect of Alkali Metal Atom Doping on the $CuInSe_2$-Based Solar Cell Absorber. J. Phys. Chem. C 2017, 121, 15516-15528.

[5] Chirlia, A.; Reinhard, P.; Pianezzi, F.; Bloesch, P.; Uhl, A. R.; Fella, C.; Kranz, L.; Keller, D.; Gretener, C.; Hagendorfer, H.; Jaeger, D.; Erni, R.; Nishiwaki, S.; Buecheler, S.; Tiwari, A. N. Potassium-Induced Surface Modification of $Cu(In,Ga)Se_2$ Thin Films for High-Efficiency Solar Cells. Nat. Mater. 2013, 12, 1107-1111.

[6] Jackson, P.; Wuerz, R.; Hariskos, D.; Lotter, E.; Witte, W.; Powalla, M. Effects of heavy Alkali Elements in $Cu(In,Ga)Se_2$ Solar Cells with Efficiencies up to 22.6 %. Phys. Status Solidi RRL 2016, 10, 1-4.

[7] Kato, T.; Wu, J.-L.; Hirai, Y.; Sugimoto, H.; Bermudez, V. Record Efficiency for Thin-Film Polycrystalline Solar Cells up to 22.9 % Achieved by Cs-Treated $Cu(In,Ga)(Se,S)_2$. IEEE J. Photovolt. 2019, 9, 325-330.

[8] Avancini, E.; Carron, R.; Weiss, T. P.; Andres, C.; Bürki, M.; Figi, R.; Romanyuk, Y. E.; Buecheler, S.; Tiwari, A. N. Effects of rubidium Fluoride and Potassium Fluoride Post Deposition Treatments on $Cu(In,Ga)Se_2$ Thin Films and Solar Cell Performance. Chem. Mater. 2017, 29, 9695-9704.

[9] Maticiuc, N.; Kodalle, T.; Lauche, J.; Wenisch, R.; Bertram, T.; Kaufmann, C. A.; Lauermann, I. In Vacuo XPS Investigation of $Cu(In,Ga)Se_2$ Surface After RbF Post Deposition Treatment. Thin Solid Film 2018, 665, 143-147.

[10] Huang, F. Q.; Deng, B.; Ellis, D. E.; Ibers, J. A. Preparation, Structures, and Band Gaps of $RbInS_2$ and $RbInSe_2$. J. Solid State Chem. 2005, 178, 2128-2132.

[11] Kodalle, T.; Kormath Madam Raghupathy, R.; Bertram, T.; Maticiuc, N.; Yetkin, H. A.; Gunder, R.; Schlatmann, R.; Kühne, T.; Kaufmann, C. A.; Mirhosseini, H. Properties of $RbInSe_2$ Thin Films. Phys. Status Solidi RRL 2019, 13, 1800564.

[12] Kresse, G.; Furthmüller, J. Efficiency of Ab-Initio Total Energy Calculations for Metals and Semiconductors Using a Plane-Wave Basis Set. Comput. Mater. Sci. 1996, 6, 15-50.

[13] Perdew, J. P.; Burke, K.; Ernzerhof, M. Generalized Gradient Approximation Made Simple. Phys. Rev. Lett. 1996, 77, 3865-3868.

[14] Bloechl, P. E. Projector Augmented-Wave Method. Phys. Rev. B 1994, 50, 17953.

[15] Fonari, A.; Stauffer, S. Raman Off-Resonant Activity Calculator Using VASP as a Back-End, vasp_raman.py. https://github.com/raman-sc/VASP/ (accessed December 19, 2019).

[16] Bouchenafa, M.; Sidoumou, M.; Halit, M.; Benmakhlouf, A.; Bouhemadou, A.; Maabed, S.; Bentabet, A.; Bin-Omran, S. Theoretical Investigation of the Structural, Elastic, Electronic and Optical Properties of the Ternary Indium Sulfide Layered Structures $AInS_2$ (A = K, Rb and Cs). Solid State Sci. 2018, 76, 74-84.

[17] Yuksek, N. S.; Gasanly, N. M. Temperature Dependence of Raman-Active Mode Frequencies and Linewidths in $TlGaSe_2$ Layered Crystals. Cryst. Res. Technol. 2005, 40, 264-270.

[18] Friedrich, D.; Schlosser, M.; Pfitzner, A. Synthesis and Structural Characterization of the Layered Selenogallate $RbGaSe_2$. Z. Anorg. Allg. Chem. 2017, 643, 1589-1592.

[19] Kauschke, W.; Cardona, M. Resonant Raman Scattering in Semiconductors. Phys. Scripta 1989, T25, 201-205.

[20] Schorr, S.; Gurieva, G.; Guc, M.; Dimitrievska, M.; Pérez-Rodríguez, A.; Izquierdo-Roca, V.; Schnohr, C. S.; Kim, J.; Jo, W.; Merino, J. M. Point Defects, Compositional Fluctuations and Secondary Phases in Non-Stoichiometric Kesterites. J. Phys. Energy 2019, 2, 012002.

[21] Poborchii, V. V.; Kolobov, A. V.; Tanaka, K. An In Situ Raman Study of Polarization-Dependent Photocrystallization in Amorphous Selenium Films. Appl. Phys. Lett. 1998, 72, 1167.

[22] Dimitrievska, M.; Fairbrother, A.; Fontané, X.; Jawhari, T.; Izquierdo-Roca, V.; Saucedo, E.; Pérez-Rodríguez, A. Multiwavelength Excitation Raman Scattering Study of Polycrystalline Kesterite Cu_2ZnSnS_4 Thin Films. Appl. Phys. Lett. 2014, 104, 021901.

[23] Placidi, M.; Dimitrievska, M.; Izquierdo-Roca, V.; Fontané, X.; Castellanos-Gomez, A.; Pérez-Tomás, A.; Mestres, N.; Espindola-Rodriguez, M.; López-Marino, S.; Neuschitzer, M.; Bermudez, V.; Yaremko, A.; Pérez-Rodríguez, A. Multiwavelength Excitation Raman Scattering Analysis of Bulk and Two-Dimensional MoS_2: Vibrational Properties of Atomically Thin MoS_2 Layers. 2D Mater. 2015, 2, 035006.

[24] Vidal-Fuentes, P.; Guc, M.; Alcobe, X.; Pérez-Rodríguez, A.; Saucedo, E.; Izquierdo-Roca, V. Multiwavelength Excitation Raman Scattering Study of Sb_2Se_3 Compound: Fundamental Vibrational Properties and Secondary Phases Detection, 2D Mater. 2019, 6, 045054.

[25] Bottcher, P. Darstellung und Kristallstruktur der Dialkalimetall-trichalkogenide Rb_2S_3, Rb_2Se_3, Cs_2S_3 und Cs_2Se_3. Z. Anorg. Allg. Chem. 1980, 461, 13-21. /In German/

[26] Bottcher, P. Synthesis and Crystal Structure of the Dirubidiumpentachalcogenides Rb_2S_5 and Rb_2Se_5. Z. Kristallogr. 1979, 150, 65-73.

[27] Syrotyuk, S. V.; Shved, V. M. Quasiparticle Electronic Band Structure of the alkali Metal Chalcogenides. Condens. Matter Phys. 2015, 18, 33702.

[28] Xie, H.-H.; Ma, R.-Y.; Gao, Q.; Li, L.; Deng, J.-B. Half-Metallic Ferromagnetism of RbSe and CsTe Compounds: A Density Functional Theory Study. Chem. Phys. Lett. 2016, 661, 89-93.

[29] Kambas, K.; Julien, C.; Jouanne, M.; Likforman, A.; Guittard, M. Raman Spectra of α- and γ-In_2Se_3. Phys. Stat. Sol. B 1984, 124, K105-K108.

[30] Lewandowska, R.; Bacewicz, R.; Filipowicz, J.; Paszkowicz, W. Raman Scattering in α-In_2Se_3 Crystals. Mater. Res. Bull. 2001, 36, 2577-2583.

[31] Weszka, J.; Daniel, Ph.; Burian, A.; Burian, A. M.; Nguyen, A. T. Raman Scattering in In_2Se_3 and $InSe_2$ Amorphous Films. J. Non-Cryst. Solid 2000, 265, 98-104.

[32] de Groot, C. H.; Moodera, J. S. Growth and Characterization of a Novel In_2Se_3 Structure. J. Appl. Phys. 2001, 89, 4336-4340.

[33] Balitskii, O. A.; Savchyn, V. P.; Yukhymchuk, V. O. Raman Investigation of InSe and GaSe Single-Crystals Oxidation. Semicond. Sci. Technol. 2002, 17, L1-L4.

[34] Berg, D. M.; Arasimowicz, M.; Djemour, R.; Gütay, L.; Siebentritt, S.; Schorr, S.; Fontané, X.; Izquierdo-Roca, V.; Pérez-Rodriguez, A.; Dale, P. J. Discrimination and Detection Limits of Secondary Phases in Cu_2ZnSnS_4 Using X-Ray Diffraction and Raman spectroscopy. Thin Solid Film 2014, 569, 113-123.

[35] Nam, D.; Lee, J.-U.; Cheong, H. Excitation Energy Dependent Raman Spectrum of $MoSe_2$. Sci. Rep. 2015, 5, 17113.

[36] Rissom, T.; Kaufmann, C. A.; Caballero, R.; Schniebs, J.; Schock, H.-W.; Wiedenbeck, M. Influence of Mo Back-Contact Oxidation on Properties of $CIGSe_2$ Thin Film Solar Cells on Glass Substrates. Jpn. J. Appl. Phys. 2012, 51, 10NC02.

[37] Theelen, M.; Harel, S.; Verschuren, M.; Tomassini, M.; Hovestad, A.; Barreau, N.; Berkum, J.; Vroon, Z.; Zeman, M. Influence of $Mo/MoSe_2$ Microstructure on the Damp Heat Stability of the $Cu(In,Ga)Se_2$ Back Contact Molybdenum. Thin Solid Film 2016, 612, 381-392.

[38] Ren, Y.; Richter, M.; Keller, J.; Redinger, A.; Unold, T.; Donzel-Gargand, O.; Scragg, J. J. S.; Platzer Björkman, C. Investigation of the SnS/Cu_2ZnSnS_4 Interfaces in Kesterite Thin-Film Solar Cells. ACS Energy Lett. 2017, 2, 976-981.

[39] Kondrotas, R.; Colina, M.; Guc, M.; Neuschitzer, M.; Giraldo, S.; Alcobé, X.; Oliva, F.; Sánchez, Y.; Pistor, P.; Izquierdo-Roca, V.; Pérez-Rodriguez, A.; Saucedo, E. Towards In-Reduced Photovoltaic Absorbers: Evaluation of Zinc-Blende $CuInSe_2$-ZnSe Solid Solution. Sol. Energy Mater. Sol. Cell 2017, 160, 26-33.

[40] Giraldo, S.; Saucedo, E.; Neuschitzer, M.; Oliva, F.; Placidi, M.; Alcobe, X.; Izquierdo-Roca, V.; Kim, S.; Tampo, H.; Shibata, H.; Perez-Rodrıguez, A.; Pistor, P. How Small Amounts of Ge Modify the Formation Pathways and Crystallization of Kesterites. Energy Environ. Sci. 2018, 11, 582-593.

[41] Caballero, R.; Haass, S. G.; Andres, C.; Arques, L.; Oliva, F.; Izquierdo-Roca, V.; Romanyuk, Y. E. Effect of Magnesium Incorporation on Solution-Processed Kesterite Solar Cells. Front. Chem. 2018, 6, 5.

[42] Tanino, H.; Maeda, T.; Fujikake, H.; Nakanishi, H.; Endo, S.; Irie, T. Raman Spectra of $CuInSe_2$. Phys. Rev. B 1992, 45, 13323-13330.

[43] Rincon, C.; Ramirez, F. J. Lattice Vibrations of $CuInSe_2$ and $CuGaSe_2$ by Raman Microspectrometry. J. Appl. Phys. 1992, 72, 4321-4324.

[44] Izquierdo-Roca, V.; Fontane, X.; Saucedo, E.; Jaime-Ferrer, J. S.; Alvarez-Garcia, J.; Perez-Rodriguez, A.; Bermudez, V.; Morante, J. R. Process Monitoring of Chalcopyrite Photovoltaic Technologies by Raman Spectroscopy: An Application to Low Cost Electrodeposition Based Processes. New J. Chem. 2011, 35, 453-460.

[45] Kim, S. Y.; Kim, J.H. Fabrication of CIGS Thin Films by Using Spray Pyrolysis and Post-selenization, J. Kor. Phys. Soc. 2012, 60, 2018-2024.

[46] Insignares-Cuello, C.; Izquierdo-Roca, V.; Lopez-Garcia, J.; Calvo-Barrio, L.; Saucedo, E.; Kretzschmar, S.; Unold, T.; Broussillou, C.; Goislard de Monsabert, T.; Bermudez, V.; Perez-Rodriguez, A. Combined Raman Scattering/Photoluminescence Analysis of $Cu(In,Ga)Se_2$ Electrodeposited Layers. Sol. Energy 2014, 103, 89-95.